Clim Dyn (2013) 41:45–61
DOI 10.1007/s00382-012-1547-1

Intraseasonal SST-precipitation relationship and its spatial variability over the tropical summer monsoon region

Mathew Roxy · Youichi Tanimoto · B. Preethi · Pascal Terray · R. Krishnan

Received: 18 February 2012 / Accepted: 26 September 2012 / Published online: 31 October 2012

Abstract The SST-precipitation relationship in the intraseasonal variability (ISV) over the Asian monsoon region is examined using recent high quality satellite data and simulations from a state of the art coupled model, the climate forecast system version 2 (CFSv2). CFSv2 demonstrates high skill in reproducing the spatial distribution of the observed climatological mean summer monsoon precipitation along with its interannual variability, a task which has been a conundrum for many recent climate coupled models. The model also exhibits reasonable skill in simulating coherent northward propagating monsoon intraseasonal anomalies including SST and precipitation, which are generally consistent with observed ISV characteristics. Results from the observations and the model establish the existence of spatial variability in the atmospheric convective response to SST anomalies, over the Asian monsoon domain on intraseasonal timescales. The response is fast over the Arabian Sea, where precipitation lags SST by $\sim$5 days; whereas it is slow over the Bay of Bengal and South China Sea, with a lag of $\sim$12 days. The intraseasonal SST anomalies result in a similar atmospheric response across the basins, which consists of a destabilization of the bottom of the atmospheric column, as observed from the equivalent potential temperature anomalies near the surface. However, the presence of a relatively strong surface convergence over the Arabian Sea, due to the presence of a strong zonal gradient in SST, which accelerates the upward motion of the moist air, results in a relatively faster response in terms of the local precipitation anomalies over the Arabian Sea than over the Bay of Bengal and South China Sea. With respect to the observations, the ocean–atmosphere coupling is well simulated in the model, though with an overestimation of the intraseasonal SST anomalies, leading to an exaggerated SST-precipitation relationship. A detailed examination points to a systematic bias in the thickness of the mixed layer of the ocean model, which needs to be rectified. A too shallow (deep) mixed layer enhances (suppress) the amplitude of the intraseasonal SST anomalies, thereby amplifying (lessening) the ISV and the active-break phases of the monsoon in the model.

Keywords Asian summer monsoon · Intraseasonal variability · SST precipitation relationship · Ocean atmosphere interaction

M. Roxy (✉) · B. Preethi · P. Terray · R. Krishnan
Centre for Climate Change Research, Indian Institute of Tropical Meteorology, Pune 411008, India
e-mail: roxy@tropmet.res.in

Y. Tanimoto
Faculty of Environmental Earth Science and Graduate School of Environmental Science, Hokkaido University, Sapporo, Japan

Y. Tanimoto
Research Institute for Global Change, JAMSTEC, Yokohama, Kangawa, Japan

P. Terray
Laboratoire d'Océanographie Dynamique et de Climatologie, IPSL, Paris, France

1 Introduction

The Asian summer monsoon, during June–September, directly affects the lives of over two billion people, which is about one-third of the world population. Despite the recent advances in research and development, and strategic shifts in agricultural methods, the summer monsoon variability over the Asian continent is still an important limiting factor for stable food production, and thus for social and economic development in these regions (Tao et al.

2004; Gadgil and Gadgil 2006; Gadgil and Rupa Kumar 2006). A major aspect of the monsoon variability, usually playing the decisive role on the agricultural sector, is its intraseasonal variability (ISV) which manifests as active and break spells of precipitation over the Asian monsoon region (Goswami and Ajayamohan 2001). ISV of the Asian summer monsoon is characterized by a broadband spectrum with periods ranging from 10 to 90 days, but have two preferred bands, one between 10 and 20 days with a westward or north-westward propagation pattern over the monsoon region and the other from 30 to 60 days which exhibits a northward or north-eastward propagation (Yasunari 1979, 1980; Krishnamurti and Ardanuy 1980; Krishnamurti and Subrahmanyam 1982; Murakami et al. 1984; Lau and Peng 1987; Goswami and Ajayamohan 2001; Krishnamurthy and Achuthavarier 2012). Though the two timescales have different origins and implications, they interact with each other and together they influence the active and break phases of the monsoon (Mao and Chan 2005). No attempt to separate the different timescales embedded within the ISV is done in the current study because, as far as the "local" SST-precipitation relationship is concerned, both the timescales are found to contribute to it.

Sea surface temperature (SST) and surface heat flux anomalies associated with the ISV, are observed over a large zonal domain, extending from the Arabian Sea to the South China Sea and even to the western North Pacific, evident through the active and break phases of the monsoon (Webster et al. 1998; Sengupta et al. 2001; Vecchi and Harrison 2002; Xie et al. 2007). SST has high intraseasonal variability in these tropical oceans, especially the Bay of Bengal and the South China Sea (Sengupta et al. 2001). Studies based on observations (e.g: Roxy and Tanimoto 2007, 2012; Joseph and Sabin 2008; Wu 2010) and numerical experiments (e.g: Fu et al. 2008) have suggested a significant influence of intraseasonal SST anomalies on the atmospheric variability, over the north Indian Ocean and the north-western portion of the tropical Pacific. On the other hand, there is increasing evidence that atmospheric changes contribute to SST anomalies in these regions, highlighting the coupled nature of the climate in these regions (Hendon and Glick 1997; Roxy and Tanimoto 2007; Wu 2010).

Over the tropical oceans higher SSTs are generally accompanied by increased precipitation (Trenberth and Shea 2005; Vecchi and Harrison 2002). Roxy and Tanimoto (2007, 2012), using satellite data, examined the processes involved in the SST-precipitation relationship over the monsoon domain, and found that the underlying positive SST anomalies induce unstable conditions in the lower atmosphere and enhance the precipitation anomalies. They observed that the northward propagating (at a speed of 0.9° latitudes day^{-1}) positive SST anomalies lead the positive surface air temperature (SAT) anomalies, which are followed by the positive $\Delta\theta_e$ anomalies (difference between the equivalent potential temperatures at 1,000 and 700 hPa), suggesting the active role of SST anomalies in destabilizing the lower atmosphere, a condition favorable for enhanced convective activity. Several studies have examined the spatial variability in the evolution mixed layer and surface temperatures over the Indo-Pacific oceans with respect to the atmospheric forcing (e.g: Duvel et al. 2004; Duvel and Vialard 2007; Vialard et al. 2011). In comparison, the present study examines the spatial variability of the SST-precipitation relationship, with respect to the oceanic forcing. Roxy and Tanimoto (2007, 2012) carried out individual analysis on the SST-precipitation over these basins, but never examined the differences in the temporal response of precipitation to the intraseasonal SST anomalies over these basins.

The overall objective of the present study, hence, is to understand the background mechanism for the inter-basin variability of the air-sea interaction, with a comparison of observations and a state-of-the-art model. Though the ocean-to-atmosphere effect regulating the co-variability between intraseasonal SST and precipitation anomalies is similar over the Arabian Sea, Bay of Bengal and the South China Sea, different lead-lag relationships are observed in these regions (Vecchi and Harrison 2002; Roxy and Tanimoto 2007, 2012; Wu 2010). Understanding the ocean–atmosphere processes regulating the time response and intensity of the SST-precipitation co-variability is crucial for evaluating and rectifying (coupled) model forecasts (Wu et al. 2006, 2008). For example, Wu et al. (2008) using local SST-precipitation relationship found discrepancy between their ocean–atmosphere coupled model and observations with an SST lag time longer in the model than in observations. This was attributed to a slower SST response to atmospheric changes in the model, as compared to observations. It is possible that different regional factors, including the differences in the ocean–atmosphere interaction over these regions are contributing to the pronounced spatial variability in the SST-precipitation relationship. The first objective of the present study, hence, is to examine the contrasting SST-precipitation relationship over the monsoon region and to explore the processes involved in it. Since the SST-precipitation relationship is a significant factor in modulating the model forecast, the analysis is carried out both in observations and a state-of-the-art coupled model.

Though the ISV is a dominant factor of the monsoon, past climate models, including those in the IPCC AR4 (Fourth Assessment Report of the Intergovernmental Panel on Climate Change) array had significant biases in simulating the intraseasonal variability over the tropics (Lin et al. 2006; Lau et al. 2012). Since the last IPCC exercise,

the climate modeling scene has advanced, with improvements in the physics of the models, including modifications in the ocean–atmosphere coupling, convection schemes and radiation parameterizations of the model. Data assimilation techniques for providing the initial conditions have also improved (e.g: Saha et al. 2010). This calls for a re-examination of how well current state-of-the-art models can simulate the monsoon ISV, and hence, our second objective. For examining the ocean-atmospheric processes involved in the ISV of the Asian monsoon, we use the climate forecast system version 2 (CFSv2; Saha et al. 2010), a coupled general circulation model (CGCM), recently introduced by the National Centre for Environment Prediction (NCEP). Hence the second objective of the current study is to serve as a validation of the ISV of the SST-precipitation relationship in the CFSv2, for the Asian monsoon region.

In the rest of the paper, Section 2 presents the observed data, model and methodology used in the present study. In Sect. 3, the model mean state and ISV during boreal summer monsoon are validated and examined thoroughly. The variability of ISV across the different tropical ocean basins, embedded in the tropical monsoon region at similar latitudes is then examined and the associated ocean-atmospheric processes are explored. Section 4 summarizes the results and discusses their implications, including suggestions for improving the CFSv2 and similar coupled models for a much more realistic simulation of the ISV.

2 Data, model and analysis methods

2.1 Data

Examining and validating the ISV requires high quality datasets with high resolution both in the temporal and spatial domains. Hence a suite of new high resolution satellite observations of SST, winds, and precipitation and objective analysis of latent heat and shortwave fluxes, which are available since the last decade, are utilized in the present study. The 3-day running mean SST and precipitation based on the TRMM Microwave Imager (TMI), and sea surface winds from the microwave scatterometer on the QuikSCAT satellite merged with the data from the European Remote Sensing (ERS) scatterometer, on a $\sim 0.25°$ grid are used. The surface latent heat flux (SLHF) and the downward shortwave radiation flux (DSWRF) are obtained from the TropFlux project version 1(Praveen Kumar et al. 2012), which on comparison with fluxes from the global tropical moored array shows a better performance than NCEP, NCEP2 or ERA-interim re-analyses, and a similar performance to the OAFlux product (Yu et al. 2008). The satellite and observed fields are supplemented with daily air temperature and specific humidity at 1.5° grid based on the European Centre for medium-range weather forecasts (ECMWF) Interim (ERA-Interim) reanalysis. Considering the availability of all these variables across the recent years, data from 1998 to 2009 (12 years) are used in the present study.

2.2 Model

The climate forecast system (CFSv2) is a fully coupled ocean–land–atmosphere-sea ice model from the National Centre for Environment Prediction (NCEP), with significant improvements since its first version (CFSv1; Saha et al. 2006, 2010). This version of the CFSv2 is similar to the version of the NCEP model used for the NCEP climate forecast system Reanalysis (CFSR; Saha et al. 2010; Wang et al. 2011). The atmospheric component of the CFSv2 is the NCEP Global Forecast System (GFS) model. It adopts a spectral triangular truncation of 126 waves (T126) in the horizontal ($\sim 0.9°$ grid) and a finite differencing in the vertical with 64 sigma-pressure hybrid layers. The convection scheme employed in GFS is the Simplified Arakawa-Schubert (SAS) convection, with cumulus momentum mixing and orographic gravity wave drag (Saha et al. 2010). The land surface model (LSM) used in CFSv2 is the Noah LSM, with 4 layers (Ek et al. 2003). See Saha et al. (2010) for further details on the NCEP GFS.

The ocean component is the Modular Ocean Model version 4p0d (MOM4p0d; Griffies et al. 2004), from the Geophysical Fluid Dynamics Laboratory (GFDL), which is a finite difference version of the ocean primitive equations configured under the Boussinesq and hydrostatic approximations. The zonal resolution is 0.5° and the meridional resolution is 0.25° between 10°S and 10°N, becoming gradually coarser through the tropics, up to 0.5° poleward of 30°S and 30°N. There are 40 layers in the vertical with 27 layers in the upper 400 m, with a bottom depth of approximately 4.5 km. The vertical resolution is 10 m from the surface to the 240-m depth, gradually increasing to about 511 m in the bottom layer. Vertical mixing in the ocean component is based on the K-profile parameterization scheme (KPP; Large et al. 1994). The ocean model is coupled with an interactive, 3 layered sea-ice model, an interactive GFDL Sea Ice Simulator. Further details of the MOM4p0d can be found in Griffies et al. (2004).

The atmosphere, ocean, land and sea ice exchange quantities such as the heat and momentum fluxes every half an hour, with no flux adjustment or correction. The CFSv2 model is time integrated over a period of 100 years, and the simulated daily data is used in the present study for examining the ISV. In the model simulation the mixing ratios of time varying forcing agents such as atmospheric CO_2, CH_4, N_2O, etc. are set for the current decade ($\sim$ year

2009), so that the model climate is comparable with the observed climate from the recent high resolution data.

2.3 Methodology

The equivalent potential temperature (θ_e) of an air parcel increases with increasing temperature and moisture content. The vertical profile of θ_e may be used as a measure of vertical stability of the lower atmospheric column (Roxy and Tanimoto 2007). As an illustration, a decrease (increase) in θ_e with altitude may lead to unstable (stable) atmospheric conditions, which can increase (decrease) the local convection. The lower tropospheric air temperature and specific humidity from ERA interim reanalysis are used to derive the equivalent potential temperature (θ_e).

Data of SST, precipitation and all other variables are interpolated to daily for compatibility among the observed variables, before statistical analysis. Intraseasonal anomalies are then obtained for all variables by removing the seasonal means and band pass filtering in the 10–90 days band to retain all the significant intraseasonal signals over the Asian monsoon region, for both the observations and the model.

3 Results

3.1 Simulation of the summer monsoon in the model

Before examining the monsoon ISV in the observations and the model, it is important to examine how well the model simulates the Asian summer monsoon climate. Figure 1a and b show the mean precipitation for June–September over the monsoon region, in the observations and the model. The mean patterns of the observed monsoon precipitation appear to be well simulated in the model. Over the land, the model precipitation is realistic over the Western Ghats (west coast of India) and the Himalayas, and reasonably simulated over the central and northeastern India, east coast of China, and coastal regions surrounding the South China Sea. Precipitation over the sea is also well simulated, especially over the Bay of Bengal, though there is some overestimation over the Arabian Sea and the South China Sea. In comparison with other state-of-the-art coupled models in terms of the mean summer monsoon, this is a significant advancement, as even getting the precipitation distribution over the monsoon domain has been difficult across the several recent coupled ocean–atmosphere circulation models (Kripalani et al. 2007; Preethi et al. 2010; Terray et al. 2011). For example, many of these models overestimate the precipitation over the central Indian Ocean, whereas the CFSv2 has a better simulation over this region (Terray et al. 2011). This is a significant progress, and possibly denotes that the Indian monsoon is better resolved and the ocean–atmosphere coupling and northward propagating ISV has improved in the present model, in comparison with earlier models, especially the CFSv1 (Chaudhari et al. 2012; Pokhrel et al. 2012; Samala et al. 2012). Resolving the diurnal cycle of SST through high frequency coupling in the model also might have contributed to the improvement in the ocean-atmospheric coupling, even with a 10 m vertical resolution in the upper ocean, consistent with some recent studies using other coupled models (Mujumdar et al. 2011; Terray et al. 2011; Masson et al. 2012). Figure 1c and d show the mean SST for June–September over the tropical monsoon domain, in the observations and the model. The spatial distribution of SST including the meridional and zonal gradients, and the upwelling regions along the west coast of Arabian Sea are well simulated in the model, though the mean SST has a cold bias of about 1 $\sim$ 3 °C over the tropical ocean, which is a shortcoming common to many CGCMs (Roxy et al. 2011).

To quantify the model's skill in reproducing spatial pattern of precipitation climatology, pattern correlation between the precipitation simulated by the model and observations is computed (Table 1). The correlations are computed over four different domains, the Arabian Sea (63–73°E), Bay of Bengal (85–95°E) and the South China Sea (110–120°E) over similar latitudes (5–20°N) and over the Indian subcontinent (70–90°E, 10–30°N) where the northward propagating intraseasonal anomalies are active. The model shows very high skill over the Arabian Sea and Bay of Bengal ($r = 0.83$ and 0.8), high skill over the South China Sea ($r = 0.7$) and moderate skill ($r = 0.6$) over the subcontinent. This indicates a high skill for the model in simulating the spatial pattern of summer precipitation over the monsoon domain.

In terms of interannual variability of the summer monsoon precipitation over the Arabian Sea, the model shows a climatological precipitation rate of 4 mm day^{-1} with a standard deviation of 1 mm day^{-1} giving a coefficient of variation (the variability in relation to the mean) of 24 %, while these statistics are, respectively, 2.4 mm day^{-1}, 0.7 mm day^{-1} and 29 % for the observations. Over the Bay of Bengal, these values are 9.6 mm day^{-1}, 0.75 mm day^{-1} and 7.8 % for the model, and 8.4 mm day^{-1}, 0.74 mm day^{-1} and 8.8 % for the observations, respectively. For the South China Sea, the model has a climatological precipitation rate of 10.4 mm day^{-1} with a standard deviation of 0.9 mm day^{-1} and coefficient of variation 8.5 %, while it is 7.7 mm day^{-1}, 0.77 mm day^{-1} and 10 % for the observations. The precipitation rate and variability in the model are on par with those in the observations. The Arabian Sea shows comparatively higher coefficient of variation, both in the observations and the model, implying a

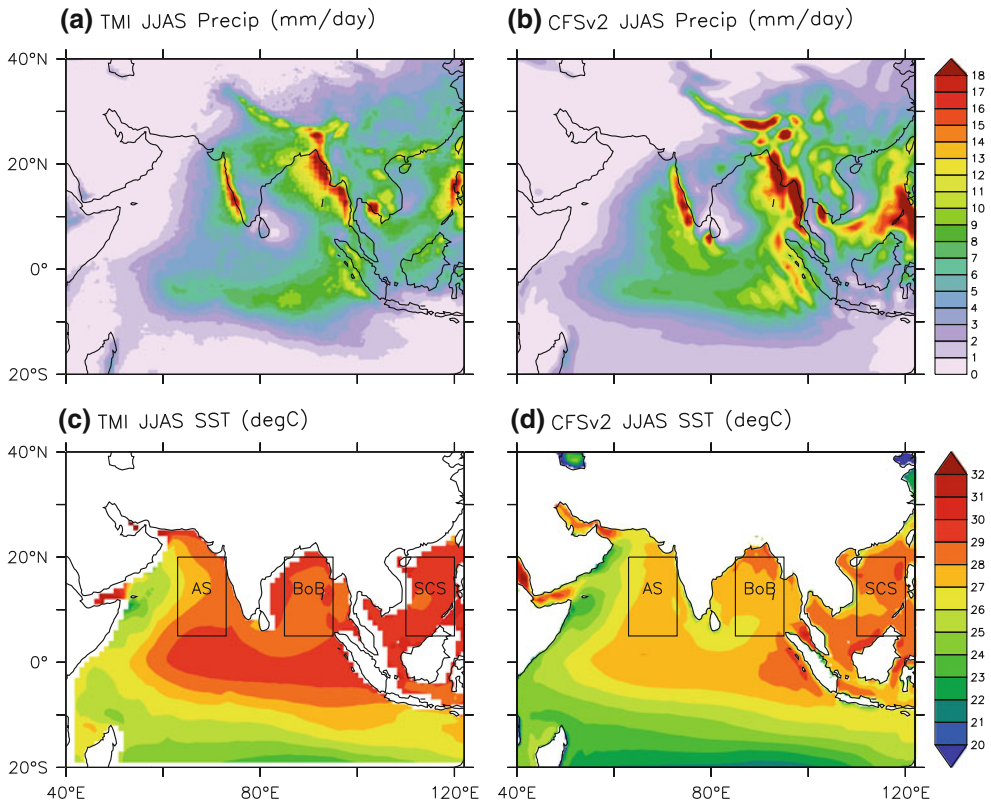

Fig. 1 Climatology of precipitation (*colors*; mm day^{-1}) and SST (*colors*; °C) over the Asian monsoon region during June–September, for (**a**, **c**) the observations (1998–2009) and (**b**, **d**) the model (100 years run). *Shading* conventions are represented at the side of the figures. The *inset rectangles* represent the regions under consideration, for the present study

Table 1 Mean monsoon and variability, TMI vs CFSv2

	AS	BoB	SCS
TMI			
Mean (mm day^{-1})	2.4	8.4	7.7
SD (mm day^{-1})	0.7	0.74	0.77
C.V.	29 %	8.8 %	10 %
CFS2			
Mean (mm day^{-1})	4	9.6	10.4
SD (mm day^{-1})	1	0.75	0.9
C.V.	24 %	7.8 %	8.5 %
TMI versus CFS2 pattern correlation	0.83	0.8	0.7

relatively stronger interannual variability of the summer monsoon over the region. Over the Indian subcontinent, the quantities are 5 mm day^{-1}, 0.85 mm day^{-1} and 18 % for the model, and 7.3 mm day^{-1}, 0.8 mm day^{-1} and 11.5 % for the observations, respectively. Over the subcontinent, the coefficient of variation is lower for the model, implying a weaker monsoon interannual variability over the land in comparison with the observations.

3.2 Spatial variability of intraseasonal SST-precipitation relationship over the monsoon region

To elucidate the intraseasonal SST-precipitation relationship in the observations and the model, the lead-lag correlations of the precipitation anomalies with respect to the SST anomalies at the intraseasonal time scale over the Arabian Sea, Bay of Bengal and the South China Sea are estimated from 20 days before to 20 days after, and shown in Figs. 2a and b. A positive (negative) correlation observed when precipitation lags (leads) the SST anomalies indicates that the SST (atmosphere) is driving the atmosphere (SST), identified as an ocean-to-atmosphere (atmosphere–to-ocean) effect (Roxy and Tanimoto 2007, 2012; Wu 2010). The magnitude of the correlation refers to the intensity of the driving force, and the corresponding lag (lead) time denotes how quickly the atmosphere responds to the SST anomalies and vice versa. A short lag (lead) in precipitation, coupled with a large maximum (minimum) correlation, indicates a strong SST (atmospheric) forcing. A regression analysis of the anomalies (figure not shown) gives similar results as in Figs. 2a and b. However, the correlation coefficients are utilized in this study for comparing the ocean atmosphere interactions over the basins,

as correlation is symmetric while regression is not. This is useful if we want to assess the strength of the coupling without implying a causal relationship. Though some studies using monthly data emphasize the nonlinearity in the SST-precipitation relationship, especially when SST increases beyond 28 and 29.5 °C (Gadgil et al. 1984; Rajendran et al. 2012), other studies show that precipitation can consistently increase even at higher temperatures, and that any apparent decrease is likely influenced by large-scale subsidence forced by nearby or remotely generated deep convection (Lau et al. 1997; Su et al. 2003). In the present study, the local intraseasonal SST-precipitation relationship with their respective lead-lags factored in shows weak nonlinearity, where the error of linear fit is about 10 %. Hence, a correlation of SST and precipitation is used as a measure of the linear association between the two variables.

The local SST-precipitation relationship appears to show a spatial variability over the Asian monsoon region, in the observations (Fig. 2a). Precipitation lags SST by ~5 days over the Arabian Sea while the lag is ~12 days over the Bay of Bengal and the South China Sea. That is, the ocean-to-atmosphere effect appears to be fast over the

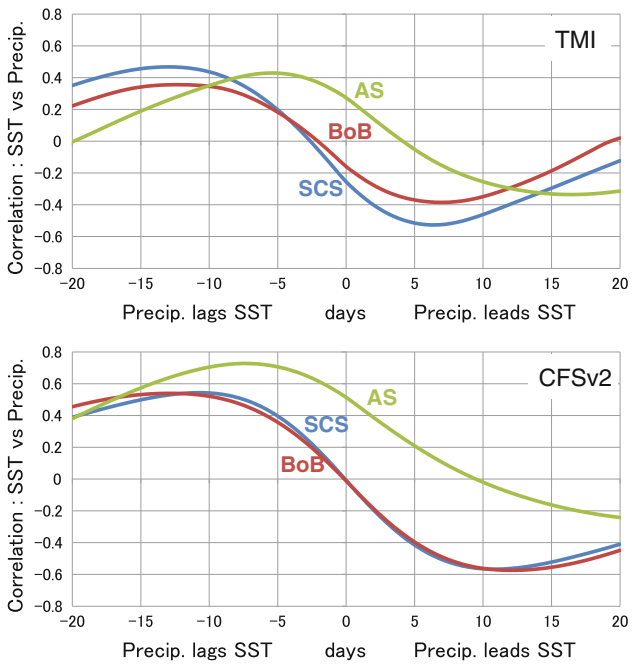

Fig. 2 Lead-lag correlation of precipitation anomalies with respect to SST anomalies, on intraseasonal time scales averaged over the Arabian Sea (*AS*), Bay of Bengal (*BoB*) and the South China Sea (*SCS*), based on the *inset rectangles* in Fig. 1. A positive (negative) correlation observed when precipitation lags (leads) the SST anomalies indicates that the SST (atmosphere) is driving the atmosphere (SST), identified as an ocean-to-atmosphere (atmosphere–to-ocean) effect. The magnitude of the correlation refers to the intensity of the driving force, and the corresponding lag (lead) time denotes how quickly the atmosphere responds to the SST anomalies and vice versa

Arabian Sea, whereas the effect is slow over the other two regions. Meanwhile, the atmosphere-to-ocean effect is slower over the Arabian Sea (~15 days), with a quicker response observed over the Bay of Bengal and the South China Sea (~7 days). Such a substantial difference in the SST-precipitation relationship between the regions is striking as they are located at similar latitudes with similar large-scale monsoon circulation characteristics like the southwesterly winds, and to some extent, exhibits intra-seasonal variability on similar timescales and northward propagating nature. Despite these similarities, Duvel et al. (2004) noted that, on regional scales, features including the cloud cover, mixed layer depth and even the phase and speed of propagation of the ISV over these basins are different. Duvel and Vialard (2007) examined the evolution of the ISV of the mixed layer temperature over the Indo-Pacific region with respect to the atmospheric convection. They found that during the boreal summer the SST response to convective activity and surface wind perturbations are regulated by the mixed layer depth over these regions. In a recent study, Vialard et al. (2011) examined the evolution of SST over the tropical Indian Ocean using an ocean general circulation model and suggested a spatial variability in the evolution of SST anomalies over the Indian Ocean. They suggested that wind-stress variations contribute to a larger extent to the intraseasonal SST variations in the Arabian Sea through modulation of oceanic processes such as vertical mixing, entrainment, lateral advection and Ekman pumping, whereas surface heat flux variations contribute more to the ISV of SST over the Bay of Bengal. However, their study focuses on the ISV over the western Arabian Sea (48–60°E) in the Somalia and Oman upwelling regions, where the coastal ocean dynamics play a major role in the evolution of the SST anomalies. In contrast, Roxy and Tanimoto (2007) examined the evolution of intraseasonal SST over the central Arabian Sea (60–70°E) and Bay of Bengal (85–95°E), away from the influence of the coastal upwelling processes, and showed that the surface fluxes play a dominant role in generating the observed intraseasonal SST anomalies in these regions. The studies by Duvel and Vialard (2007) and Vialard et al. (2011) focus on the spatial variability in the evolution of mixed layer and surface temperatures in response to atmospheric and oceanic drivers. The present study proceeds further into analyzing the evolution of the SST-precipitation relationship and the dynamical processes involved, over these regions. Domains similar to those in Roxy and Tanimoto (2007) are utilized in the current study, were the large scale monsoon circulation is similar, and the surface fluxes dominate the ISV of SST, rather than processes such as the coastal dynamics, entrainment and advection, and focus on the significant differences in the response of precipitation to the intraseasonal SST

anomalies. Though the intraseasonal anomalies and its propagation is observed over the other regions such as the western north Pacific, these regions are excluded as the surface winds are not south westerly, and hence the large scale monsoon features are different.

The coupled model simulates many aspects of the observed spatial variability in the SST-precipitation relationship (Fig. 2b). This renders some confidence in the model in portraying the ISV over the monsoon domain as far as the ocean–atmosphere coupling is concerned. Though the response times are realistic over the basins, the sensitivity of the precipitation to the SST in the model is intensified, especially over the Arabian Sea. The maximum correlation between SST and precipitation for the Arabian Sea is overestimated in the model ($r = 0.7$) in comparison with the observations ($r = 0.4$, significant at the 99 % confidence levels). This disparity in SST-precipitation correlation is of some concern as it could indicate that the ocean–atmosphere coupling is intensified over the Arabian Sea, possibly influencing the mean precipitation over the region, as the ISV can significantly modulate the seasonal mean monsoon fields (Krishnamurthy and Shukla 2000; Goswami and Ajayamohan 2001). Though the timescale under consideration in the present study is 10–90 days, similar results are obtained with the anomalies filtered only for 30–60 days. It is also obvious from Fig. 3 that the dominant timescale in the ISV anomalies is 30–60 days, with an average period of $\sim$40 days. Further, the lead-lags obtained are robust in the unfiltered data as in the filtered data (figure not shown), confirming the conclusions of the current study.

The differences in the dynamical process responsible for the spatial variability in the SST-precipitation relationship, which is shown both in the observations and the model, need to be examined. Though Roxy and Tanimoto (2007, 2012) showed that positive equivalent temperature anomalies induced by positive SST anomalies lead to unstable conditions of the lower atmosphere and precipitation across the Arabian Sea, Bay of Bengal and South China Sea, it is possible that different factors, including the differences in the ocean–atmosphere interaction over these regions contribute to the pronounced spatial variability in the SST-precipitation relationship. Evaluating which process control the spatial variability of ISV might also give some clues for understanding the disparity between the observations and the model leading to an overestimation of the SST-precipitation correlation in the Arabian Sea.

In order to evaluate the differences in the SST-precipitation co-variability, the temporal evolution of SST, surface equivalent temperature (θ_e) and precipitation anomalies, with respect to an SST maximum (SST above 1 standard deviation) is examined using time-latitude plots of daily composites over the Arabian Sea, Bay of Bengal and the South China Sea, for the observations and the model (Figs. 3, 4, 5). Coherent northward propagation of all the anomalies is observed in all the cases. For all the three regions, positive SST anomalies lead to positive θ_e anomalies, via heat and moisture exchanges at the surface, thereby inducing unstable conditions over the lower atmospheric column, leading to the precipitation anomalies as in Roxy and Tanimoto (2007). In the observations, the θ_e maximum is not collocated on the same latitudes with the other anomalies, though the anomalies appear to be collocated in the model. This could probably be due to the use of the ERA data for the lower atmospheric temperature and specific humidity, along with the satellite data, which could add some uncertainty to the analysis. The SST- θ_e lag is similar across the basins, but the θ_e-precipitation lag is shorter over the Arabian Sea and longer over the Bay of Bengal and the South China Sea. This means that though the positive SST anomalies translate to positive θ_e anomalies instantaneously over all the basins, the response in the precipitation anomalies is different. For understanding the spatial variability in the ISV, it is necessary to juxtapose the results with the spatial variability of the mean conditions over these regions which can modulate the precipitation response to the unstable conditions. Surface convergence is a factor which determines the vertical motions leading to convective activity. The mean surface convergence, instead of the intraseasonal surface convergence, is used as it provides a relative measure of the spatial variability when comparing different regions. To examine the role of the mean conditions in influencing the ISV and its spatial variability, scatter plots of mean surface convergence and the response time are prepared in Figure 6, for Arabian Sea, Bay of Bengal and South China Sea, in the observations and the model. Mean surface convergence is higher over the Arabian Sea, and the response time is quicker. Meanwhile, Bay of Bengal and South China Sea have a relatively weaker surface convergence, and the response time is slower. The mean surface convergence over the Arabian Sea might be stronger due to the presence of a strong zonal gradient in SST, in comparison with the other two basins (Fig. 1). The zonal SST gradient may enhance the east–west surface pressure gradient, strengthening the westerlies, and thereby increasing the surface convergence over the region (Lindzen and Nigam 1987). The relationship between the surface convergence and the response time can be hypothesized as follows. Once the positive surface θ_e anomalies induce unstable conditions over the Arabian Sea, the prevailing strong surface convergence accelerates the vertical upward motion of the moist air, which then condenses and precipitates. In comparison, the mean surface convergence over the Bay of Bengal and South China Sea is weaker, weakening the vertical upward motion of the moist air, and

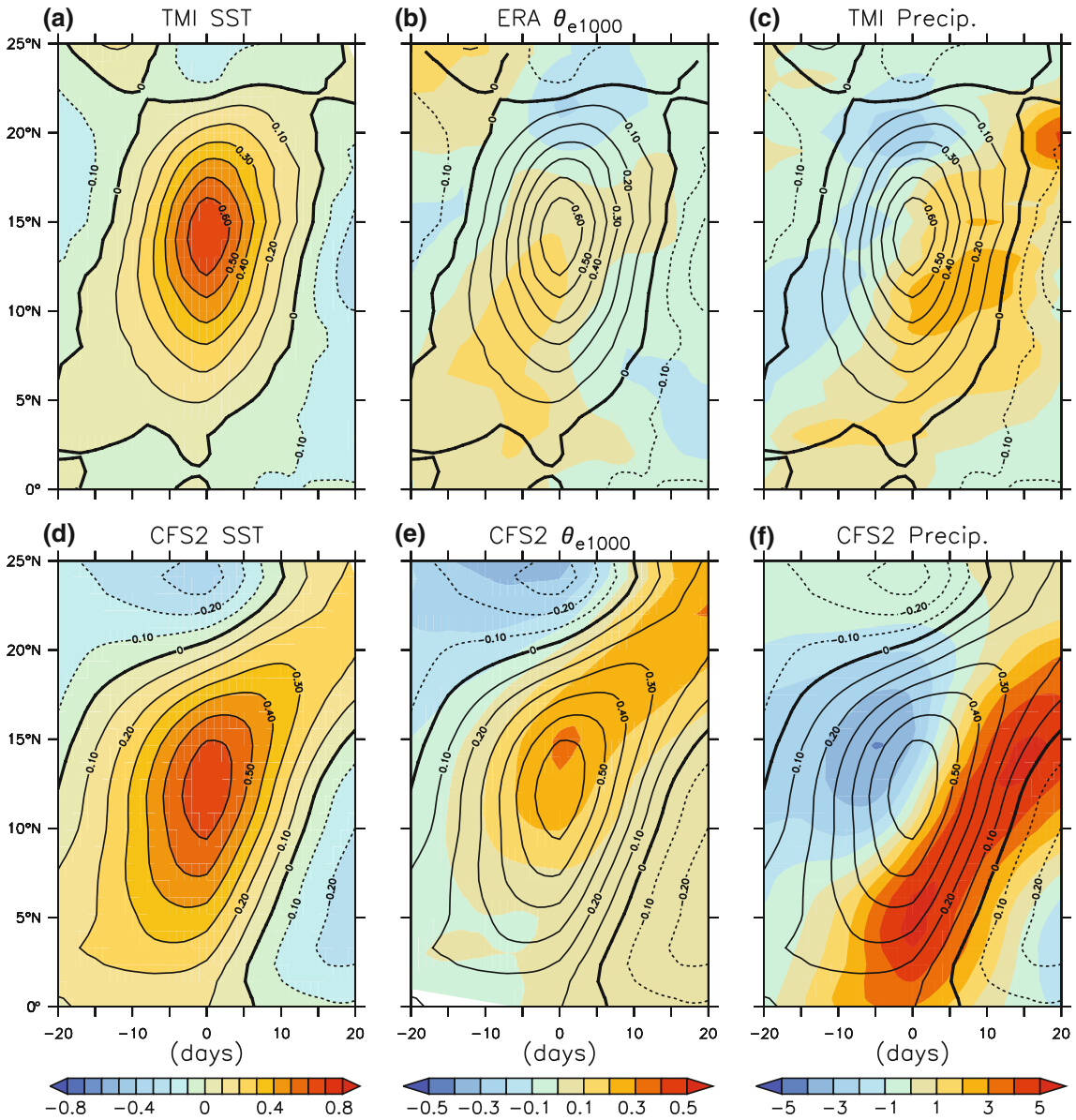

Fig. 3 Hovmoller plots of intraseasonal anomalies of SST (*colors*; °C), θ_{e1000} (*colors*; °C) and precipitation (*colors*; mm day^{-1}) over the Arabian Sea (63–73°E) with respect to the SST maximum at day = 0, for the observations and the model. Contour lines of SST anomalies (interval: 0.1 °C) are superimposed, with negative values dashed. *Coloring* convention is represented at the *bottom*

the resultant precipitation. This means that thermodynamically induced unstable conditions in the ISV requires a strong background surface convergence for a quicker response in the precipitation anomalies.

3.3 SST-precipitation relationship in the ISV of the model

The model is found to reproduce the salient features of the monsoon ISV, including its northward propagation, the SST-precipitation relationship and its co-variability (Figs. 3, 4, 5). However, there is an overestimation in the intraseasonal anomalies, leading to a stronger SST-precipitation correlation in the model with respect to the observations. As mentioned earlier, this could possibly lead to a modulation of the seasonal mean precipitation and hence requires careful evaluation. To examine the relative amplification of the ISV, the variability of all the important variables over the monsoon domains are compared between the observations and the model. Figure 7 shows the standard deviation of the ISV for the surface winds, SST and equivalent potential temperature at 1,000 hPa (θ_{e1000}) in the observations and the model. Among the observed fields, Arabian Sea shows low standard

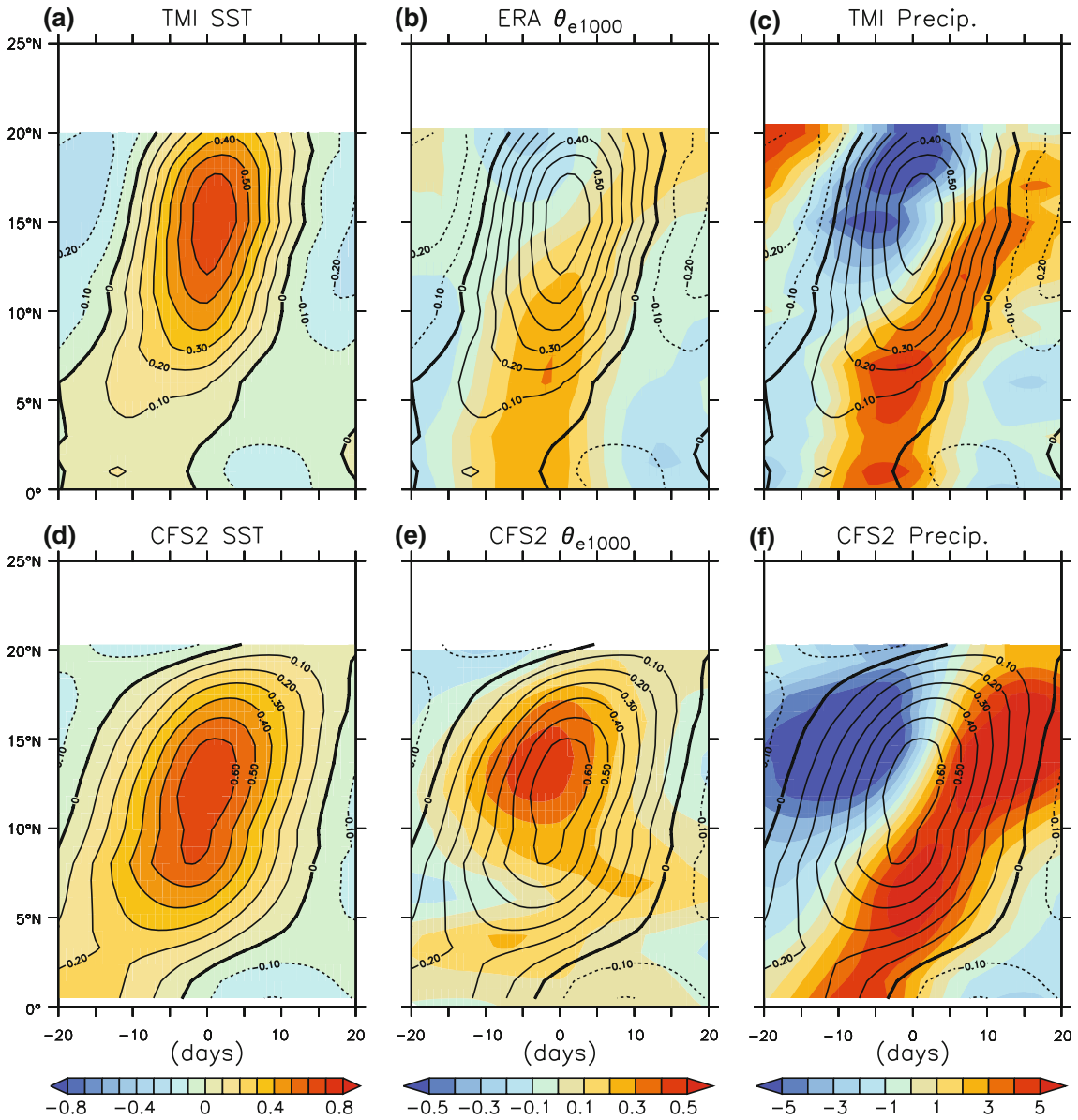

Fig. 4 Same as Fig. 3, but for the Bay of Bengal

deviations, implying weaker intraseasonal variability in comparison with the Bay of Bengal (BoB) and the South China Sea (SCS). The strong variability of equivalent potential temperature over the Bay of Bengal and South China Sea results in highly variable conditions of stability, resulting in stronger precipitation variability, as evidenced from Fig. 7. In comparison, the model has intensified ocean–atmosphere coupling over the Arabian Sea. The surface wind variability is stronger, leading to increased latent heat flux variability and in turn SST variability over the Arabian Sea. This results in the increased variability in θ_{e1000} and therefore, the precipitation in the model.

To investigate the cause of increased intraseasonal variability over the Arabian Sea in the model, it is necessary to examine the physical processes regulating the evolution of the SST anomalies at the intraseasonal time scale in more detail. First, it is important to check whether the increased SST anomalies are due to enhanced surface flux and wind variability. Figure 8 shows the latitude-time plots of daily composites of surface winds, latent heat flux and shortwave radiation flux anomalies, with respect to the SST maximum in the Arabian Sea, for both the observations and the coupled model. Northward propagation of the zonal wind, latent heat and shortwave flux (downward positive) anomalies, consistent with the evolution of the SST anomalies at the intraseasonal time scale are evident in these Hovmoller diagrams for the observations. CFSv2 produces coherent patterns in northward propagating

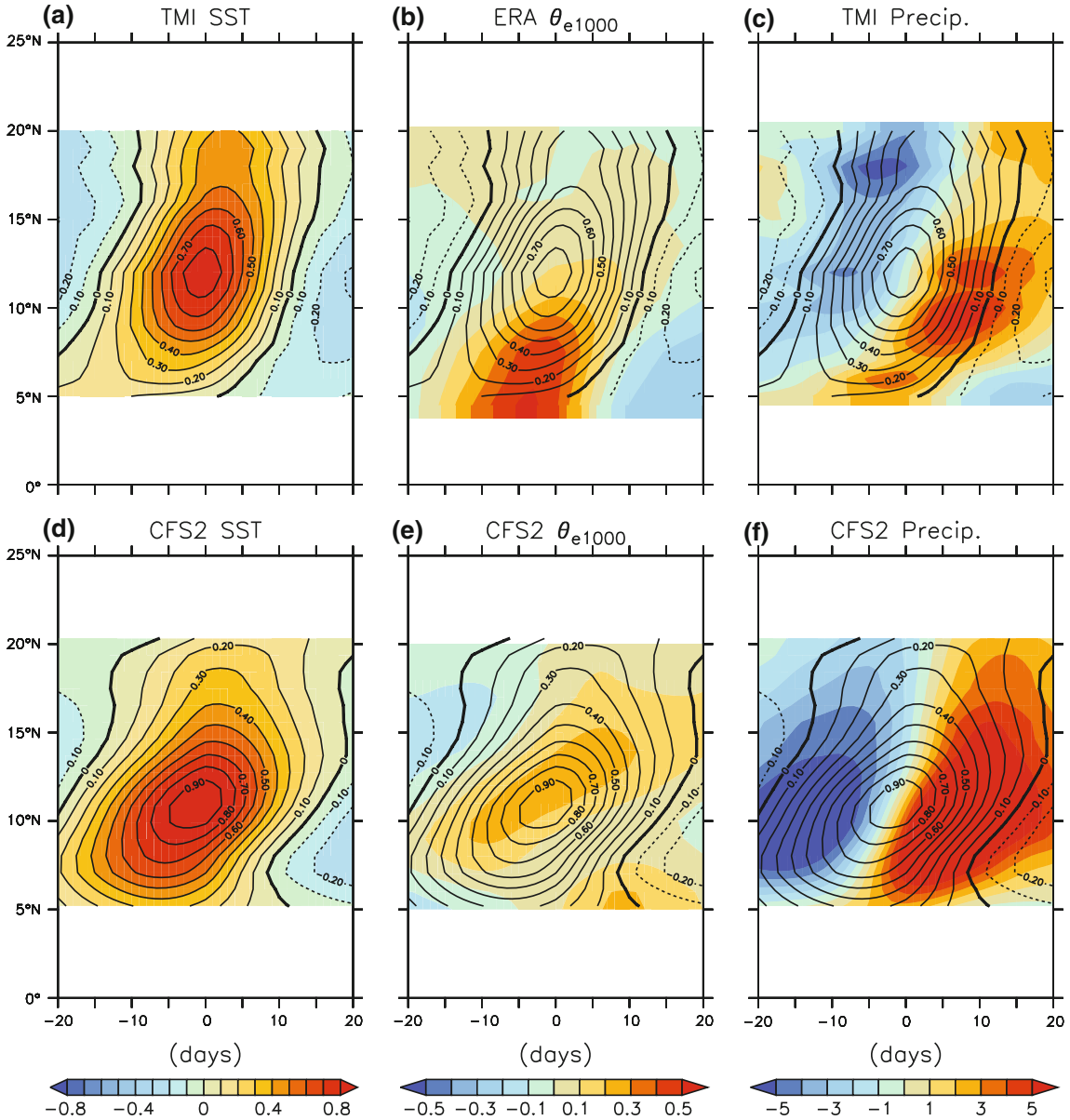

Fig. 5 Same as Fig. 3, but for the South China Sea

intraseasonal anomalies in the Arabian Sea that are generally consistent with ISV characteristics in the observations. However, the intraseasonal anomalies are in general, overestimated in the model. To assess whether this overestimation is due to poor ocean–atmosphere coupling or misrepresented coupling coefficients in the model for the monsoon domain, the anomalies are quantitatively evaluated for their contribution with respect to the increased intraseasonal SST anomalies. The increased SST anomalies in the model are comparable to the simulated net surface flux anomalies, as an increase of 30 W m^{-2} for an average mixed layer depth of 30 m corresponds to an increase of 0.025 °C day^{-1}, on estimating the surface flux contribution to the SST tendency (Roxy and Tanimoto 2012; see "Appendix 1"). The surface easterly anomalies are also magnified in the model with respect to the observations, leading to reduced evaporation (as the mean winds are westerly) and the intensified surface latent heat flux anomalies (positive downward). For example, using the bulk aerodynamic equations, an overestimation of 1 m s^{-1} of wind speed is comparable to an increase of 14 W m^{-2} of latent heat flux anomalies, in the model (see the "Appendix 2" for a detailed derivation of the quantities). The surface shortwave flux anomalies are probably intensified due to suppressed convective activity during the precipitation minimum (Fig. 3f), resulting in the anomalous easterlies (Matsuno 1966; Gill 1980; Wang and Wu 1997). An objective analysis of the results indeed shows a

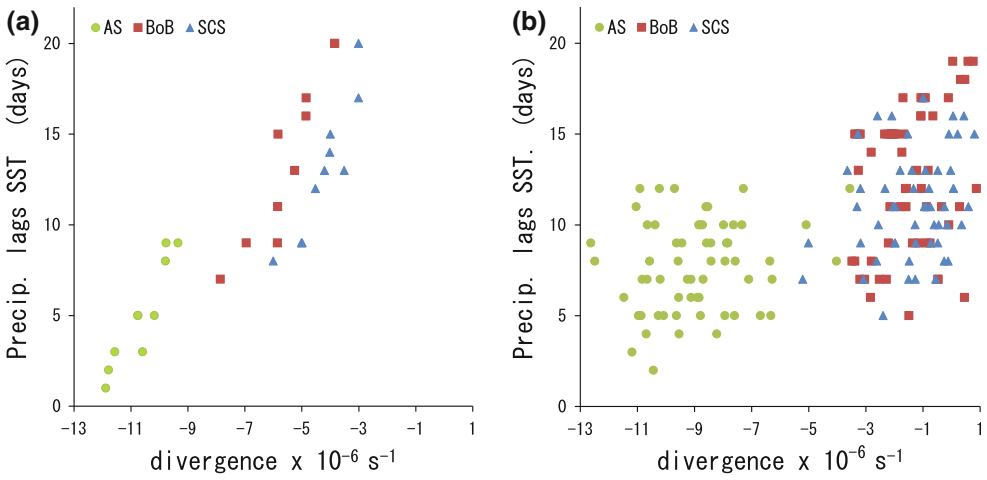

Fig. 6 Scatter plots of the SST—precipitation response time (days) with respect to surface convergence (divergence) over the Arabian Sea (AS; *green dot*), Bay of Bengal (BOB; *red square*) and South China Sea (SCS; *blue triangle*) for the (**a**) observations and (**b**) model. The lag time denotes how quickly the atmosphere responds to the SST anomalies

correlation between the simulated convective activity and the winds, though a quantitative estimation of the same is not feasible with the current study.

In summary, the ocean–atmosphere coupling at the intraseasonal time scale seems to be overestimated in the model. However, it is important to note that there is no apparent mismatch across the coupling variables, indicating that the dynamical processes involved in the air-sea coupling are fairly well represented in the model. This is different from the problem faced by some of the earlier models which simulates relatively weak SST variability and a systematic phase mismatch between surface winds, SST and precipitation, resulting in an unrealistic simulation of the coupling at the intraseasonal time scale (Xavier et al. 2008).

The overestimation of the ISV in the present model might be related to a persistent systematic bias in the ocean component of the model. In comparison with the observations, SST and MLD have a bias in the model. The model SST is cooler by about 1–3 °C over the north Indian Ocean and the South China Sea during the boreal summer (Fig. 1). For testing the role of model SST bias in modulating the ISV, model sensitivity experiments, with and without the SST bias were carried out. Ensembles of short integrations for the summer monsoon were performed by adding temperature anomalies to correct the bias on the top levels of the ocean similar to the method utilized by Terray et al. (2007). The composites of the simulations with the bias corrections in SST alone (figure not shown) did not show an improvement in simulating the ISV over the Asian monsoon region. It appears that the whole upper layer mixing in the model needs to be examined, rather than the SST exclusively. Indeed, Duvel and Vialard (2007) showed that the intraseasonal SST anomalies are related to the changes in the MLD over the Indo-Pacific region. Hence an analysis of the model response to the mixed layer depth is carried out.

Mean mixed layer depth, based on a density criteria, as in de Boyer Montégut et al. (2004) is estimated for the model and compared. In comparison with the observations, the mean mixed layer depth over the Arabian Sea is relatively shallow in the model (Fig. 9). Therefore, when forced with the same surface heat flux anomalies, larger SST anomalies will occur, enhancing the unstable conditions over the Arabian Sea, eventually resulting in an enhanced ISV of precipitation. The situation is much easier to understand by estimating the SST tendency with regard to the surface heat fluxes. Suppose a region over the Arabian Sea is forced with intraseasonal surface heat fluxes of 40 W m^{-2}. At a mixed layer depth of 40 m, the SST tendency would be 0.5 °C day^{-1} ("Appendix 1"). The same, region, at a mixed layer depth of 20 m, will exhibit an SST tendency of 0.25 °C day^{-1}. That is, a shallow mixed layer aggravates the SST anomalies, thereby amplifying the ISV over the region. Indeed, comparing the spatial patterns of the ISV in the observations and the model (Fig. 7), with the bias in the mixed layer depth (Fig. 9) shows an increase in the variance over the shallow regions of Arabian Sea. A pattern correlation is carried out between the bias in the mean mixed layer depth and the bias in the ISV of SST, over the Arabian Sea, including the regions of both shallow and deep mixed layer biases. Positive correlation ($r = 0.5$) significant at 95 % confidence levels is obtained, confirming the results from the present study. The same processes can be attributed to the Bay of Bengal and South China Sea also, where the mixed layer is shallow for the model (Fig. 9), resulting in a slight amplification of the ISV over these regions. Considering that the values of fluxes and SST estimated here are averaged over a larger region, the localized impact over a grid point could be higher, and hence significant to be factored in while examining the monsoon ISV.

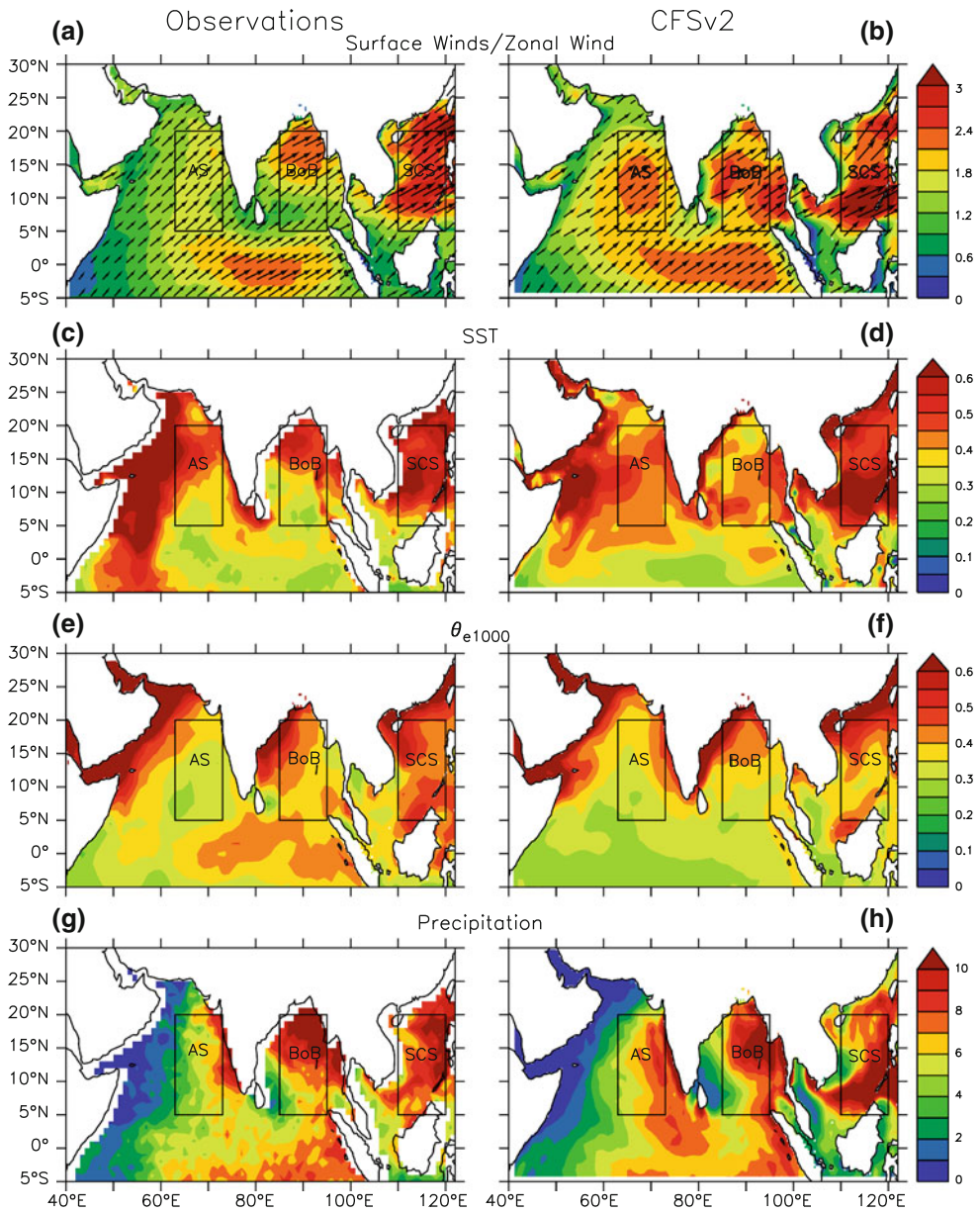

Fig. 7 Standard deviation of the intraseasonal variability of surface zonal winds (*colors*; m s^{-1}), SST (colors; °C), θ_{e1000} (*colors*; °C) and precipitation (*colors*; mm day^{-1}) over the Asian monsoon region during June–September, for the model (100 years run) and the observations (1998–2009). *Shading* conventions are represented at the side of the *figures*. Standard deviation of intraseasonal surface wind vectors are superimposed on the surface zonal wind anomalies

4 Summary and discussion

The intraseasonal variability of the Asian monsoon and the local SST-precipitation relationship inherent to it are examined in the present study, using recent high quality satellite data (12 years) and climate data simulated by a state of the art coupled model, the climate forecast system version 2 (100 years). The mixing ratios of time varying forcing agents such as atmospheric CO_2, CH_4, N_2O, etc. are set for the current decade, so that the model climate is comparable with the observed climate from the satellite data.

The local intraseasonal SST-precipitation relationship appears to show a spatial variability over the Asian monsoon region, both in the observations and the CFSv2 model. The ocean-to-atmosphere effect appears to be quick over the Arabian Sea where precipitation lags SST by $\sim$5 days; whereas the effect is slow over the Bay of Bengal and the South China Sea, with a lag of $\sim$12 days. The reason for the spatial variability is hypothesized as follows. Though the Arabian Sea, Bay of Bengal and the South China Sea exhibit similar monsoon circulation features and processes of intraseasonal ocean atmosphere

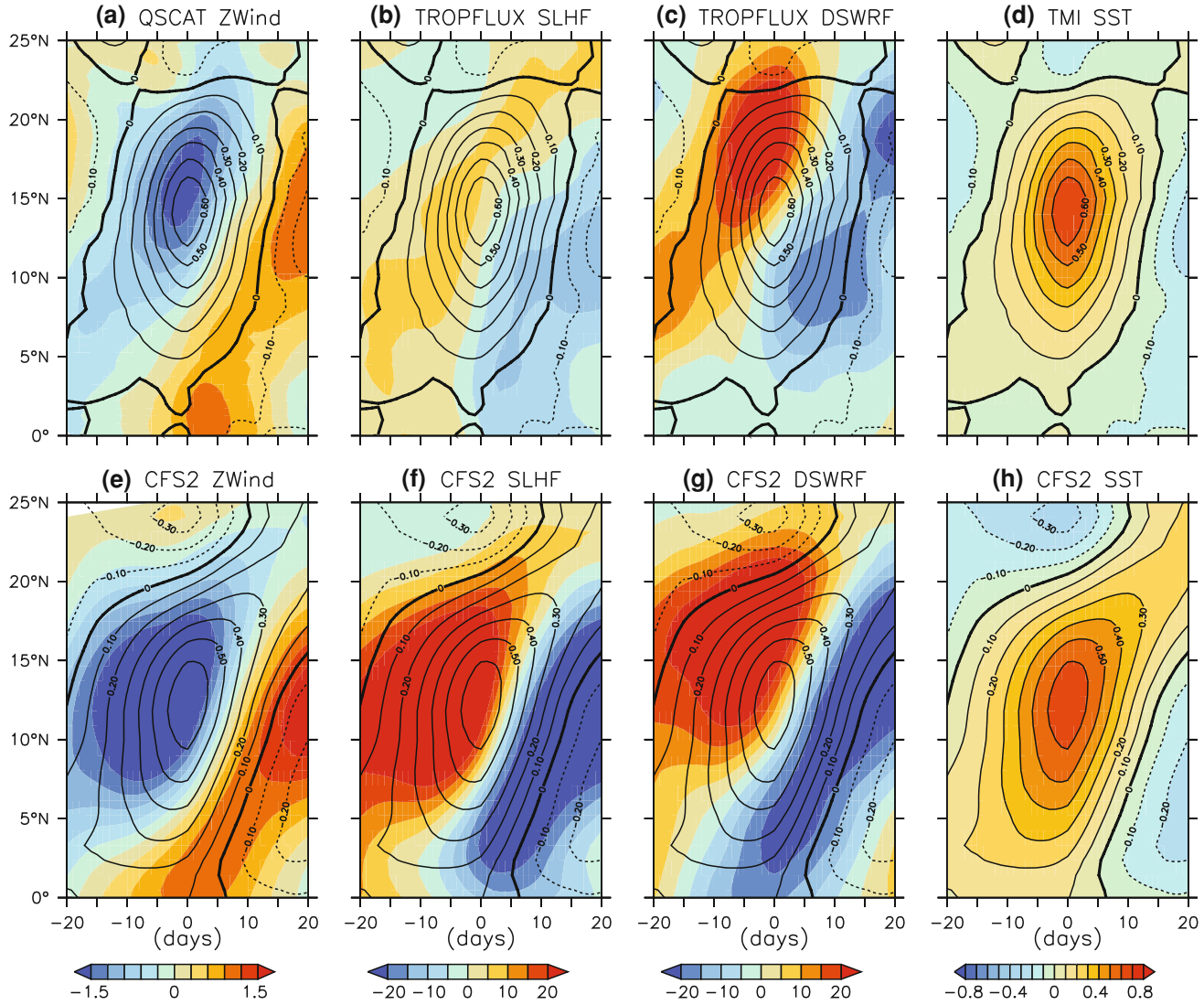

Fig. 8 Hovmoller plots of intraseasonal anomalies of surface zonal winds (*colors*; m s^{-1}), surface latent heat flux anomalies (*colors*; W m^{-2}), downward shortwave radiation flux anomalies (*colors*; W m^{-2}) and SST (*colors*; °C) over the Arabian Sea (63–73°E) with respect to the SST maximum at day = 0, for the observations and the model. Contour lines of SST anomalies (interval: 0.1 °C) are superimposed, with negative values *dashed*. *Coloring* convention is represented at the *bottom*

interaction, the precipitation anomalies over the Arabian Sea shows a relatively quicker response to the SST anomalies. This is because the relatively stronger surface convergence over the Arabian Sea, due to the presence of a strong zonal gradient in SST, accelerates the uplift of the moist air resulting in a relatively faster response in the local precipitation anomalies. Similarly, the response in the precipitation anomalies is relatively slower over the Bay of Bengal and South China Sea as these basins have a comparatively weaker surface convergence, resulting in a slower response with respect to the ISV.

Simulating the ocean–atmosphere coupling inherent to the ISV, and its characteristics including the spatial variability is of paramount significance as it contributes to the wet and dry spells of the monsoon and in turn, its interannual variability. Nevertheless, most climate models fail to reproduce the salient features of the monsoon ISV. In this context, the CFSv2 produces coherent, and consistent patterns in northward propagating intraseasonal anomalies in the Arabian Sea that are generally consistent with ISV characteristics. However, the intraseasonal anomalies are in general, amplified in the model. Since the overestimation of the magnitude of the anomalies is evident in all aspects of the ocean–atmosphere coupling instead of an amplified mismatch between the variables, it can be implied that the coupling is well simulated in the model.

This leads to the question whether the systematic bias over the Arabian Sea in the model could attribute to the amplification of the ISV over the region. The mixed layer is shallower in the north Indian Ocean, with the shallowest

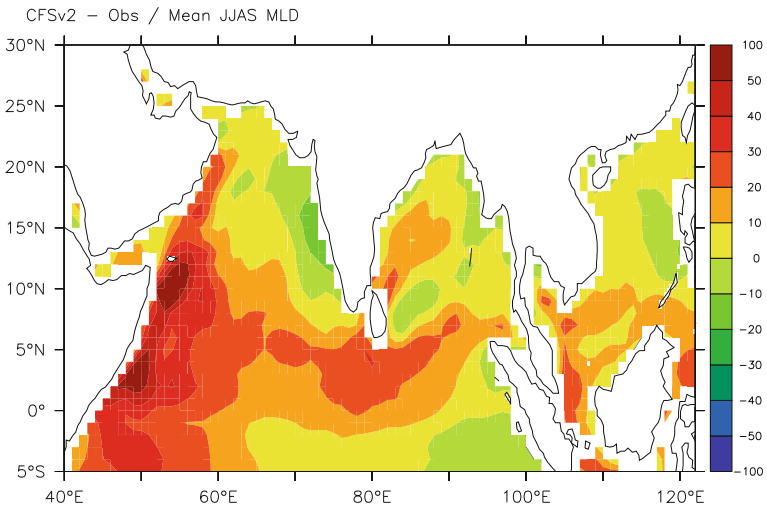

Fig. 9 Difference between the CFSv2 and the observations for the mixed layer depth (MLD, *colors*; m) over the Asian monsoon region during June–September. For the observations, MLD is obtained from de Boyer Montégut et al. (2004). *Shading* convention is represented at the side of the *figure*

regions in the Arabian Sea. When forced with the same surface flux anomalies, a shallower mixed layer will aggravate the coupled processes, leading to the increased variance of the convective activity in the model. The same mechanism can be applied to the Bay of Bengal and South China Sea also, where the mixed layer is shallow in the model, resulting in the slight amplification of the ISV over these regions. This is of a huge concern for monsoon related research and forecast, as it means that if the model does not have the mean mixed layer at the right depth, it will not reproduce the intraseasonal variability realistically, especially its amplitude. As simulating the ISV accurately is important for predicting the active and break spells of the monsoon, it is argued that a prime focus should be on improving the mixed layer scheme of the ocean component in CFSv2. The improvement may be applicable to other state-of-the-art couple models also, since the mixed layer biases are common across several of them, as mixing schemes employed are similar. With the hypotheses and propositions provided here, the SST-precipitation relationship in the active-break phases of ISV over the Asian monsoon domain is illustrated in Fig. 10, with modifications to the processes explained by previous studies (e.g: Roxy and Tanimoto 2012). To summarize, the previous studies explain how the heat fluxes increase (decrease) the SST anomalies, which in turn results in unstable (stable) lower atmospheric conditions, thereby enhancing (decreasing) convective activity. The present study supplements the previous studies, and shows that the mixed layer has a major role in regulating the amplitude of the SST anomalies and thereby the intensity of the intraseasonal variability. The current study also examines the time response of precipitation anomalies to the SST anomalies and indicates that the strength of the mean surface convergence over a basin results determine how fast or slow the response is.

The results here are in agreement with the findings of Fu et al. (2003), where they examined the relative importance of the mixed layer in determining the strength of the ISV, using numerical experiments with an ocean–atmosphere coupled model. Similar experiments for the equatorial eastward propagating Madden-Julian oscillations also showed a strengthening of the ISV with respect to shallow mixed layer depths, adding confidence to the results in the present study (Watterson 2002). Ocean–atmosphere feedbacks can amplify even small biases, and in combination with approximations in the model physics, can then affect the simulation of intraseasonal variability (Wittenberg et al. 2006). The bias in the Arabian Sea is a common issue across several models and might be an issue with the ocean component in simulating the mean mixed layer depth and the SST over the tropics (Wittenberg et al. 2006; Wu et al. 2008; Levine and Turner 2011). Levine and Turner (2011), using coupled and atmosphere-only model simulations, indicates that improving the Arabian Sea bias in the current model could possibly improve the summer monsoon and its variability. The bias in the mixed layer might be related to the KPP mixing scheme which is widely used in ocean models, including the current MOM4p0. Some physical processes such as Langmuir circulation and wave-induced vertical mixing have not been properly included in the ocean component, which could be one of the reasons for these biases. Surface waves could deliver mixing/turbulences to depth of the order of 100 m directly (Babanin et al. 2009). Langmuir circulation can induce vertical mixing and play an important role in deepening upper-ocean mixed layer. Besides Langmuir circulation and surface wave breaking, nonbreaking surface waves can also induce vertical mixing in the upper-ocean. Incorporating wave induced mixing in the KPP scheme might be a way to reduce the mixed layer bias, as shown by Shu et al. (2011). A detailed examination on the role of wave induced mixing on the present model is left for future research.

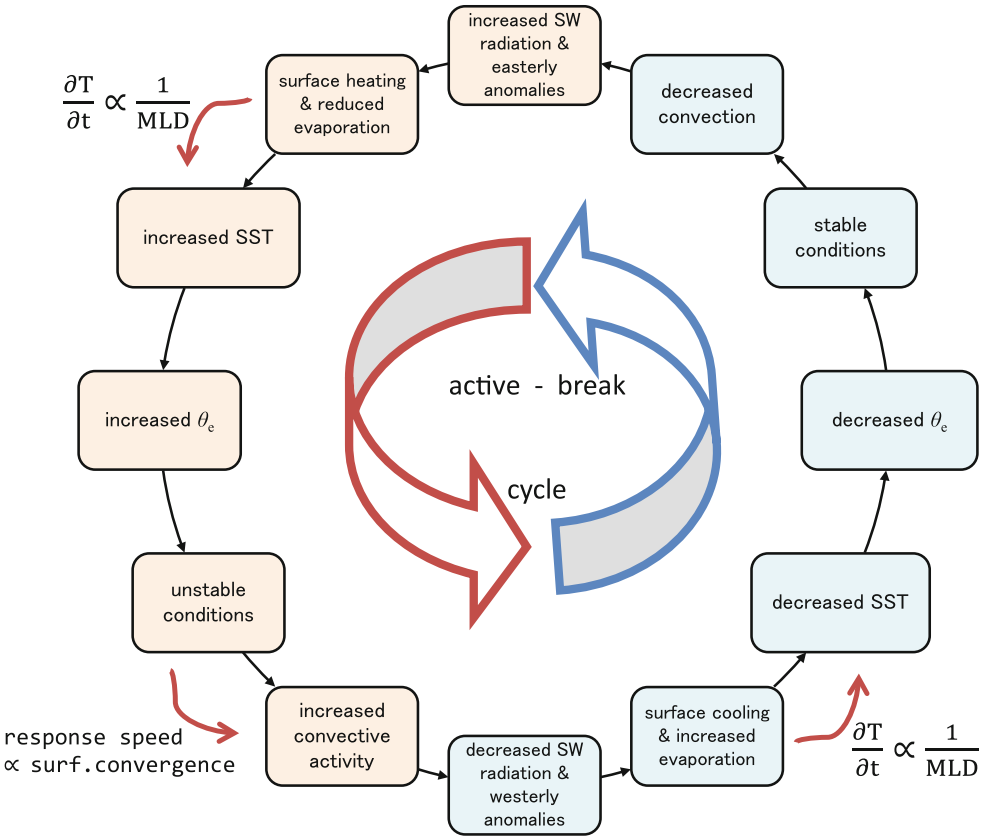

Fig. 10 A schematic figure of the SST-precipitation relationship in the active (*red shades*)—break (*blue shades*) phases of the intraseasonal variability over the tropical monsoon domain, with factors determining the spatial variability and magnitude of the relationship alongside. θ_e represents equivalent potential temperature, as a measure of vertical stability of the lower atmospheric column

The present study indicates that a bias in the mixed layer over the Indian Ocean significantly modulates the local ISV and the ocean–atmosphere coupling associated with it. It can be hypothesized that such a modulation of the ISV could modulate the precipitation over the land also. To understand this, take the case when a region over the Arabian Sea is forced with the same amount of intraseasonal surface heat fluxes, but for shallow and deep mixed layer depths. Since the latent heat flux is same, the amount of moisture evaporated to the atmosphere would be the same in both cases. However, since the ISV is amplified for a shallow mixed layer, the precipitation anomalies are also amplified, utilizing more of the moisture present over the Arabian Sea. This might reduce the amount of moisture available for precipitation over the land, in the northward and north-eastward propagating intraseasonal anomalies. However, this hypothesis is based in the assumption that moisture is a limiting factor for the intraseasonal precipitation, and hence it needs to be tested using model sensitivity experiments, and is left for future study.

Regardless of the issues discussed here, the model has the capability to serve as an excellent tool for understanding and predicting intraseasonal variations, and for investigating its response on the climate system. The simulations show robust, northward propagating intraseasonal anomalies of SST, surface winds and precipitation along the monsoon domain, which is in good qualitative agreement with observations. Difficulties in simulating the climatological mean summer monsoon, without the recurring biases in precipitation distribution over the central Indian Ocean are also resolved in the model. This may be due to a better simulation of the northward propagating ISV, as the convective bands shift to the north, and cease to persist over the central Indian Ocean. The magnitude of the ISV is found to vary with respect to the mixed layer biases in the model, with serious implications on the variability of local and northward propagating precipitation anomalies, which indicates that the biases in the model needs to be corrected for a realistic simulation of the active and break phases of the Asian monsoon.

Acknowledgments Constructive suggestions and comments from two anonymous reviewers have helped in improving the manuscript. NASA/GSFC is thankfully acknowledged for TMI/QuickScat satellite data. The surface flux data is obtained from the TropFlux Project and the lower atmospheric parameters from the ERA Interim Reanalysis. Support from NCEP in providing the CFSv2 model, through the National Monsoon Mission, is acknowledged. CFSv2 model runs and analysis were carried out at the Indian Institute of Tropical Meteorology, Ministry of Earth Sciences, India. This work was supported in part by Grand-In-Aid for Scientific Research defrayed by the Ministry

of Education, Culture, Sports, Science and Technology of Japan (22340132, 22340135, 22106007).

Appendix 1

The extent to which the surface heat flux anomalies can account for the observed intraseasonal variations of SST were examined using the SST tendency equation

$$\frac{\partial T_s}{\partial t} = \frac{F_{tot}}{\rho C_p h}$$

where T_s is the SST, F_{tot} is the total heat flux, ρ is density of water, c_p is the specific heat of water at constant pressure, and h is the mixed layer depth (MLD). In the present study, an increase of F_{tot} by 30 W m^{-2}, for an h of 30 m and standard values of ρ (1.024 gcm^{-3}) and c_p (3.898 Jg^{-1} $°C^{-1}$), the heat flux forcing estimated is in the order of 0.25 °C day^{-1}. This is comparable to the increased SST variability simulated by the model.

Appendix 2

The contribution of the increased surface winds to the increased surface latent heat flux anomalies is estimated using the bulk aerodynamic equation,

$$LHF = \rho L C_E U (q_s - q)$$

where ρ is the density of air, L is the latent heat of evaporation of water, C_E is the bulk transfer coefficient for latent heat flux, U and q are the wind speed and specific humidity of air at a height just above the surface (e.g: 10 m), and q_s is the saturation specific humidity at sea surface temperature. With respect to the present study, an overestimation of 1 m s^{-1} of wind speed, at standard values of L (2,360 Jg^{-1}), ρ (1.17 g cm^{-3}), C_E (1.25×10^3) approximated for the Indian Ocean, and a specific humidity difference dq of 4 g kg^{-1} is comparable to an increase of latent heat flux anomalies by 14 W m^{-2}, in the model.

References

Babanin AV, Ganopolski A, Phillips WRC (2009) Wave-induced upper-ocean mixing in a climate model of intermediate complexity. Ocean Model 29(3):189–197

Chaudhari HS, Pokhrel S, Saha SK, Dhakate A, Yadav R, Salunke K, Mahapatra S, Sabeerali C, Rao SA (2012) Model biases in long coupled runs of NCEP CFS in the context of Indian summer monsoon. Int J Climatol. doi:10.1002/joc.3489

de Boyer Montégut C, Madec G, Fischer AS, Lazar A, Iudicone D (2004) Mixed layer depth over the global ocean: an examination of profile data and a profile-based climatology. J Geophys Res 109(C12):12003

Duvel JP, Vialard J (2007) Indo-Pacific sea surface temperature perturbations associated with intraseasonal oscillations of tropical convection. J Clim 20(13):3056–3082

Duvel JP, Roca R, Vialard J (2004) Ocean mixed layer temperature variations induced by intraseasonal convective perturbations over the Indian Ocean. J Atmos Sci 61(9):1004–1023

Ek M, Mitchell K, Lin Y, Rogers E, Grunmann P, Koren V, Gayno G, Tarpley J (2003) Implementation of Noah land surface model advances in the National centers for environmental prediction operational mesoscale Eta model. J Geophys Res 108(D22):8851

Fu XH, Wang B, Li T, McCreary JP (2003) Coupling between northward-propagating, intraseasonal oscillations and sea surface temperature in the Indian Ocean. J Atmos Sci 60(15):1733–1753

Fu X, Yang B, Bao Q, Wang B (2008) Sea surface temperature feedback extends the predictability of tropical intraseasonal oscillation. Mon Weather Rev 136(2):577–597. doi:10.1175/2007MWR2172.1

Gadgil S, Gadgil S (2006) The Indian monsoon, GDP and agriculture. Econ Polit Week 41(47):4887–4895

Gadgil S, Rupa Kumar K (2006) The Asian monsoon—agriculture and economy. In: The Asian Monsoon. Springer Praxis Books, Springer, Berlin, pp 651–683. doi:10.1007/3-540-37722-0_18

Gadgil S, Joshi NV, Joseph PV (1984) Ocean-atmosphere coupling over monsoon regions. Nature 312:141–143

Gill AE (1980) Some simple solutions for heat-induced tropical circulation. vol 106. John Wiley & Sons, Ltd, New York. doi:10.1002/qj.49710644905

Goswami BN, Ajayamohan RS (2001) Intraseasonal oscillations and interannual variability of the Indian summer monsoon. J Clim 14(6):1180–1198

Griffies SM, Harrison MJ, Pacanowski RC, Rosati A (2004) A technical guide to MOM4. GFDL Ocean Group Tech Rep 5:371

Hendon HH, Glick J (1997) Intraseasonal air-sea interaction in the tropical Indian and Pacific Oceans. J Clim 10(4):647–661

Joseph PV, Sabin TP (2008) An ocean–atmosphere interaction mechanism for the active break cycle of the Asian summer monsoon. Clim Dyn 30(6):553–566

Kripalani R, Oh J, Kulkarni A, Sabade S, Chaudhari H (2007) South Asian summer monsoon precipitation variability: coupled climate model simulations and projections under IPCC AR4. Theoret Appl Climatol 90(3):133–159

Krishnamurthy V, Achuthavarier D (2012) Intraseasonal oscillations of the monsoon circulation over South Asia. Clim Dyn 38(11):2335–2353

Krishnamurthy V, Shukla J (2000) Intraseasonal and interannual variability of rainfall over India. J Clim 13(24):4366–4377

Krishnamurti TN, Ardanuy P (1980) The 10–20-day westward propagating mode and breaks in the monsoons. Tellus 32:15–26

Krishnamurti TN, Subrahmanyam D (1982) The 30–50 day mode at 850 mb during MONEX. J Atmos Sci 39:2088–2095

Large W, McWilliams J, Doney S (1994) Oceanic vertical mixing: a review and a model with a nonlocal boundary layer parameterization. Rev Geophys 32(4):363–403

Lau KM, Peng L (1987) Origin of low-frequency (intraseasonal) oscillations in the tropical atmosphere. Part I: basic theory. J Atmos Sci 44:950–972

Lau K, Wu H, Bony S (1997) The role of large-scale atmospheric circulation in the relationship between tropical convection and sea surface temperature. J Clim 10(3):381–392

Lau WKM, Waliser DE, Sperber K, Slingo J, Inness P (2012) Modeling intraseasonal variability. In: Intraseasonal variability in the atmosphere-ocean climate system. Springer Praxis Books, Springer, Berlin, pp 399–431. doi:10.1007/978-3-642-13914-7_11

Levine RC, Turner AG (2011) Dependence of Indian monsoon rainfall on moisture fluxes across the Arabian Sea and the impact of coupled model sea surface temperature biases. Clim Dyn 1–24

Lin JL, Kiladis GN, Mapes BE, Weickmann KM, Sperber KR, Lin W, Wheeler MC, Schubert SD, Del Genio A, Donner LJ, Emori S, Gueremy JF, Hourdin F, Rasch PJ, Roeckner E, Scinocca JF (2006) Tropical intraseasonal variability in 14 IPCC AR4 climate models. Part I: Convective signals. J Clim 19(12): 2665–2690

Lindzen RS, Nigam S (1987) On the role of sea surface temperature gradients in forcing low-level winds and convergence in the tropics. J Atmos Sci 44(17):2418–2436

Mao JY, Chan JCL (2005) Intraseasonal variability of the South China Sea summer monsoon. J Clim 18(13):2388–2402

Masson S, Terray P, Madec G, Luo JJ, Yamagata T, Takahashi K (2012) Impact of intra-daily SST variability on ENSO characteristics in a coupled model. Clim Dyn 39(3–4):681–707. doi: 10.1007/s00382-011-1247-2

Matsuno T (1966) Quasi-geostrophic motions in the equatorial area. J Meteor Soc Japan 44(1):25–42

Mujumdar M, Salunke K, Rao SA, Ravichandran M, Goswami B (2011) Diurnal cycle induced amplification of sea surface temperature intraseasonal oscillations over the Bay of Bengal in summer monsoon season. Geosci Remote Sens Lett IEEE 99:206–210

Murakami T, Nakazawa T, He J (1984) On the 40–50 day oscillations during the 1979 Northern Hemisphere summer. I: phase propagation. J Meteorol Soc Jpn 62:440–468

Pokhrel S, Chaudhari H, Saha S, Dhakate A, Yadav R, Salunke K, Mahapatra S, Rao S (2012) ENSO, IOD and Indian Summer Monsoon in NCEP climate forecast system

Praveen Kumar B, Vialard J, Lengaigne M, Murty VSN, McPhaden M (2012) TropFlux: air-sea fluxes for the global tropical oceans: description and evaluation. Clim Dyn 38(7–8):1521–1543

Preethi B, Kripalani R, Krishna Kumar K (2010) Indian summer monsoon rainfall variability in global coupled ocean-atmospheric models. Clim Dyn 35(7):1521–1539

Rajendran K, Nanjundiah RS, Gadgil S, Srinivasan J (2012) How good are the simulations of tropical SST–rainfall relationship by IPCC AR4 atmospheric and coupled models? J Earth Syst Sci 121(3):595–610

Roxy M, Tanimoto Y (2007) Role of SST over the Indian Ocean in influencing the intraseasonal variability of the Indian summer monsoon. J Meteorol Soc Jpn 85(3):349–358. doi:10.2151/jmsj.85.349

Roxy M, Tanimoto Y (2012) Influence of sea surface temperature on the intraseasonal variability of the South China Sea summer monsoon. Clim Dyn 39(5):1209–1218. doi:10.1007/s00382-011-1118-x

Roxy M, Gualdi S, Drbohlav H-K, Navarra A (2011) Seasonality in the relationship between El Nino and Indian Ocean dipole. Clim Dyn 37(1):221–236. doi:10.1007/s00382-010-0876-1

Saha S, Nadiga S, Thiaw C, Wang J, Wang W, Zhang Q, Van den Dool H, Pan HL, Moorthi S, Behringer D (2006) The NCEP climate forecast system. J Clim 19(15):3483–3517

Saha S, Moorthi S, Pan HL, Wu X, Wang J, Nadiga S, Tripp P, Kistler R, Woollen J, Behringer D (2010) The NCEP climate forecast system reanalysis. Bull Am Meteorol Soc 91(8):1015–1057

Samala BK, Krishnan R, Roxy M (2012) Assessment of 1 month forecasts of weak Indian monsoons based on the NCEP climate forecast system (CFS). Meteorol Appl 19(2):189–199. doi: 10.1002/met.1331

Sengupta D, Goswami BN, Senan R (2001) Coherent intraseasonal oscillations of ocean and atmosphere during the Asian summer monsoon. Geophys Res Lett 28(21):4127–4130

Shu Q, Qiao F, Song Z, Xia C, Yang Y (2011) Improvement of MOM4 by including surface wave-induced vertical mixing. Ocean Model 40(1):42–51

Su H, Neelin JD, Meyerson JE (2003) Sensitivity of tropical tropospheric temperature to sea surface temperature forcing*. J Clim 16(9):1283–1301

Tao F, Yokozawa M, Zhang Z, Hayashi Y, Grassl H, Fu C (2004) Variability in climatology and agricultural production in China in association with the East Asian summer monsoon and El Nino Southern Oscillation. Clim Res 28:23–30

Terray P, Chauvin F, Douville H (2007) Impact of southeast Indian Ocean sea surface temperature anomalies on monsoon-ENSO-dipole variability in a coupled ocean-atmosphere model. Clim Dyn 28(6):553–580. doi:10.1007/s00382-006-0192-y

Terray P, Kamala K, Masson S, Madec G, Sahai A, Luo JJ, Yamagata T (2011) The role of the intra-daily SST variability in the Indian monsoon variability and monsoon-ENSO-IOD relationships in a global coupled model. Clim Dyn 1:647. doi:10.1007/s00382-011-1240-9

Trenberth KE, Shea DJ (2005) Relationships between precipitation and surface temperature. Geophys Res Lett 32(14):1–4

Vecchi GA, Harrison DE (2002) Monsoon breaks and subseasonal sea surface temperature variability in the Bay of Bengal. J Clim 15(12):1485–1493

Vialard J, Jayakumar A, Gnanaseelan C, Lengaigne M, Sengupta D, Goswami B (2011) Processes of 30–90 days sea surface temperature variability in the northern Indian Ocean during boreal summer. Clim Dyn 38(9–10):1901–1916

Wang B, Wu R (1997) Peculiar temporal structure of the South China Sea summer monsoon. Adv Atmos Sci 14(2):177–194. doi: 10.1007/s00376-997-0018-9

Wang J, Wang W, Fu X, Seo KH (2011) Tropical intraseasonal rainfall variability in the CFSR. Clim Dyn 38(11–12):2191–2207

Watterson I (2002) The sensitivity of subannual and intraseasonal tropical variability to model ocean mixed layer depth. J Geophys Res 107(D2):4020

Webster PJ, Magana VO, Palmer TN, Shukla J, Tomas RA, Yanai M, Yasunari T (1998) Monsoons: Processes, predictability, and the prospects for prediction. J Geophys Res Oceans 103(C7):14451–14510

Wittenberg AT, Rosati A, Lau NC, Ploshay JJ (2006) GFDL's CM2 global coupled climate models. Part III: tropical pacific climate and ENSO. J Clim 19(5):698–722

Wu R (2010) Subseasonal variability during the South China Sea summer monsoon onset. Clim Dyn 34(5):629–642. doi:10.1007/s00382-009-0679-4

Wu R, Kirtman BP, Pegion K (2006) Local air–sea relationship in observations and model simulations. J Clim 19(19):4914–4932. doi:10.1175/JCLI3904.1

Wu R, Kirtman BP, Pegion K (2008) Local rainfall-SST relationship on subseasonal time scales in satellite observations and CFS. Geophys Res Lett 35(22):L22706. doi:10.1029/2008gl035883

Xavier PK, Duvel JP, Doblas-Reyes FJ (2008) Boreal summer intraseasonal variability in coupled seasonal hindcasts. J Clim 21(17):4477–4497

Xie SP, Chang CH, Xie Q, Wang D (2007) Intraseasonal variability in the summer South China Sea: wind jet, cold filament, and recirculations. J Geophys Res 112(10):1029

Yasunari T (1979) Cloudiness fluctuation associated with the Northern Hemisphere summer monsoon. J Meteorol Soc Jpn 57:227–242

Yasunari T (1980) A quasi-stationary appearance of 30–40 day period in the cloudiness fluc-tuations during the summer monsoon over India. J Meteorol Soc Jpn 58:225–229

Yu L, Jin X, Weller RA (2008) Multidecade global flux datasets from the objectively analyzed air–sea fluxes (OAFlux). Project: latent and sensible heat fluxes, ocean evaporation, and related surface meteorological variables., vol OA-2008-01. Woods Hole Oceanographic Institution, USA